Faculty of Physics and Astronomy
University of Heidelberg

Bachelor Thesis in Physics
submitted by

Maria Christine Heinz

born in Wiesbaden (Germany)

2013

Simulation of a photon converter for the ALICE experiment

This Bachelor Thesis has been carried out by Maria Christine Heinz at
Physikalisches Institut in Heidelberg
under the supervision of
PD Dr. Klaus Reygers

Simulation of a photon converter for the ALICE experiment

During the long shutdown in 2018 ALICE detector components will be replaced. As a result, fewer photons convert into an e^+e^- pair interacting with the material of the Inner Tracking System. In order to compensate this loss a converter is simulated in this thesis providing additional material. It could be positioned between the Inner Tracking System and the Time Projection Chamber. Knowing exactly its material and geometry the systematic uncertainties of the neutral pion and the direct photon measurements would be significantly reduced.

The converter made of copper ($X_0 = 12.86$ g/cm^2) has a cylindrical shape with an inner radius of 60 cm. Three different thicknesses are simulated using two different analysis frameworks: a GEANT 3 Monte-Carlo simulation and a faster simulation based on the Bethe-Heitler energy loss of electrons. In a first step both methods are compared regarding the energy loss of electrons and positrons. There is a good agreement so that the fast simulation can be extended for further investigations. Thus, the reconstruction efficiency of neutral pions is estimated using the fast simulation. Moreover, the photon conversion probability for the three thicknesses is determined with the Monte-Carlo simulation.

Simulation eines zusätzlichen Photonkonverters im ALICE Experiment

Während des Umbaus in 2018 werden Komponenten des ALICE Detektors teilweise ausgetauscht. Als Folge dessen verringert sich der Wirkungsquerschnitt für die Paarbildung von Photonen am Inner Tracking System. Daher wird in dieser Arbeit ein Konverter simuliert, der als zusätzliches Material zwischen Inner Tracking System und Time Projection Chamber eingebaut werden könnte. Das Wissen um das Material und die geometrischen Eigenschaften dieses Bauteils würde die systematischen Unsicherheiten der Messungen von neutralen Pionen und direkten Photonen deutlich verringern.

Der Konverter besteht aus Kupfer ($X_0 = 12.86$ g/cm^2) und ist zylinderförmig mit einem Innenradius von 60 cm. Drei unterschiedliche Materialstärken werden untersucht. Dafür wird sowohl eine Monte-Carlo Simulation via GEANT 3 als auch eine schnellere Simulation, die auf der Bethe-Heitler Formel für den Energieverlust von Elektronen beruht, verwendet. In einem ersten Schritt werden in dieser Arbeit die beiden Methoden bezüglich des Energieverlusts von Elektronen und Positronen verglichen. Es zeigt sich, dass die Bethe-Heitler Formel das Verhalten beider Teilchen gut beschreibt. Dies rechtfertigt, die schnelle Simulation für weitere Analysen zu verwenden. Zusätzlich wird eine Abschätzung der Rekonstruktionseffizienz von neutralen Pionen mit Hilfe dieser Simulation vorgenommen. Außerdem wird die Konversionswahrscheinlichkeit von Photonen für die drei Materialstärken mit der Monte-Carlo Simulation bestimmt.

Contents

Appendix

1 Introduction

The ALICE experiment at CERN's Large Hadron Collider (LHC) is the only dedicated experiment for the study of the quark-gluon plasma (QGP), a state of matter which exists at very high temperatures and densities and which is assumed to have formed just after the Big Bang. For this, the most important quantities are the chiral nature of the phase transition, the number of degrees of freedom and the initial temperature. The last two features can be studied by analyzing thermal radiation which is coming from the QGP and which is expected at low transverse momentum p_T. The best reconstruction procedure for photons at low p_T is given by tracking the electron-positron pair of converted photons in the Time Projection Chamber (TPC).

By now, the greatest limitations in the reconstruction of neutral pions with the conversion method are given by the material budget uncertainty of 9% which is constant over the whole p_T range. In fact, from $p_T = 0$ GeV to $p_T = 5$ GeV it dominates all other systematic errors namely the ones of signal extraction, particle identifications and track and particle reconstruction processes. That is the reason why the reconstructed quantities like the kinematics of photons or the invariant mass of neutral pions are limited by at least 9% at the moment.

In 2018 there will be the second long shutdown. Several changes are planned concerning the setup of the detector like the upgrade of the Inner Tracking System (ITS). This directly influences the measurements of interest because the material budget in front of the TPC will be reduced by a factor of approximately 2. Thus, the probability of photon conversion is also reduced. So, implementing an external converter is of interest which could preserve the photon conversion method. In addition, the material budget would be known more accurately. As a consequence, the error due to the material would be quite small and the photon reconstruction would be improved. The main photon source are neutral pions because they are the lightest mesons. They are created in large number in collisions at LHC and decay into two photons with a branching ratio of 98.8%. Hence, their reconstruction would be improved as well.

An external photon converter made of brass has already been used at the PHENIX experiment at RHIC, USA having a radiation length of 1.7% [1]. The thickness of the converter is an important property. On the one hand, if it is too thin there is an insufficient number of photon conversions and the statistics and the π^0 invariant mass reconstruction worsens. On the other hand, if the material is too thick the resolution of the invariant mass distribution of neutral pions and the signal to background ratio get worse. For these reasons, three different thicknesses are analyzed in this thesis considering an photon converter made of pure copper, for simplicity. The converter should be positioned between the ITS and the TPC since the electrons and positrons created by pair production shall be tracked in the TPC. For the converter a cylindrical shape with an inner radius of 60 cm and a rapidity range of $|\eta| < 0.9$ is assumed according to the available space in the detector.

In the following analysis two different frameworks are used: firstly, a full Monte-Carlo simulation of the converter, using GEANT 3 which is accessible via the CERN framework *root* and secondly, a much faster simulation in which the Bethe-Heitler formula describes the expected energy loss due to the converter. With GEANT, the conversion probability of photons is investigated for the different thicknesses and the energy loss of electrons and positrons is compared to the faster simulation. The good agreement between both justifies to use the fast simulation to get a rough estimation of the π^0 reconstruction efficiency.

2 Theoretical Background

In general, a particle has several ways to interact with matter. To get a measure of the probability of each interaction the concept of a cross section is used. This quantity depends on both the particle energy and the characteristics of the material whose properties are described by the *radiation length* X_0. Both interpretations are valid: regarding electrons, X_0 is the mean distance over which the particle loses all but $\frac{1}{e}$ of its energy; regarding high-energy photons, X_0 is $\frac{7}{9}$ of the mean free path for pair production (see Section 2.1.3). For instance, the radiation length of copper is $X_0 = 12.86$ g/cm^2 [2].

2.1 Interaction of photons with matter

Photons are massless and electrically neutral particles which have a constant velocity in vacuum, the velocity of speed of light. These properties lead to mainly three possibilities to interact with matter, namely the *photoelectric effect, Compton Scattering and pair creation*, which dominate in different energy regions as it can be seen in Figure 2.1.

2.1.1 Photoelectric Effect

In a range up to several 100 keV the photoelectric effect is the main way of photons to interact with matter. Electrons are emitted of the bound shell of atoms having taken the total energy of the initial photon. Since the binding energy W_A has to be taken into account a freed, so called *photoelectron* has the kinetic energy $E_{kin} = h\nu - W_A$ with the frequency ν of the photon and the Planck constant h.

The Feynman diagram in Figure 2.2 shows that energy and momentum conservation require an atom to interact with. Therefore, the total energy cannot be transferred to free electrons. The photoelectric effect is more likely for heavy absorbers (having a large atomic number Z) and in cases in which the photon energy is similar to the binding energy of the electrons. The last condition leads to high cross sections which can be seen in Figure 2.1 as absorption edges. Comparing the cross sections of carbon and lead one can conclude that for the lighter atom carbon ($Z = 6$) electrons can only be freed from the K-shell so that one peak is visible whereas for lead ($Z = 82$) electrons from different shells absorb photons.

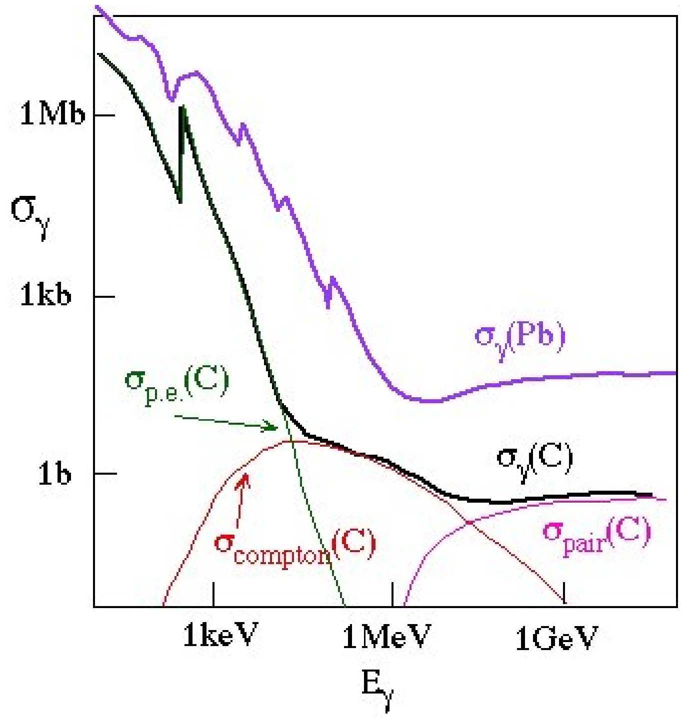

Figure 2.1: Schematic plot of the cross section σ_γ of photon interactions [3]
σ_γ(Pb): total cross section for lead
σ_γ(C): total cross section for carbon
$\sigma_{\text{p.e.}}$(C): cross section of the photoelectric effect for carbon
σ_{compton}(C): cross section of the Compton effect for carbon
σ_{pair}(C): cross section of pair production for carbon

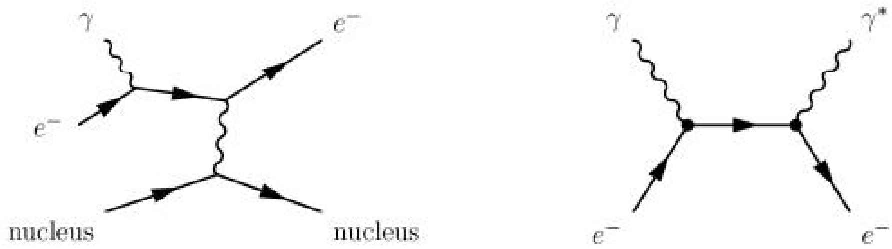

Figure 2.2: Feynman diagrams for the photoelectric effect (left) and Compton scattering (right) [4]

2.1.2 Compton Scattering

The dominant process for intermediate energies up to a few MeV is called *Compton scattering.* An incoming photon transfers a part of its energy to an electron of the medium. Therefore, it is deflected through an angle θ with respect to its original direction. The energy of the scattered photon γ^* depends on θ and has a large range since all angles are possible. It is given by

$$\frac{1}{E_{\gamma^*}} - \frac{1}{E_\gamma} = \frac{1}{m_e c^2} \cdot (1 - \cos\theta) \tag{2.1}$$

with the photon energy E_γ in the initial and E_{γ^*} in the final state, the mass of the electron m_e and the speed of light c.

2.1.3 Pair Production

If the energy of a photon E_γ is larger than $2m_e c^2 \approx 1.02$ MeV it can create an electron-positron-pair in the Coulomb field of an atom. Again, the nucleus has to take part in the interaction so that energy and momentum are conserved in this process (cf. Figure 2.3). As a consequence, the angle between the produced electron and positron is very small. Because of the increasing influence of pair production for increasing energy one can approximate a differential cross section valid for high energies.

$$\frac{\mathrm{d}\sigma}{\mathrm{d}x} = \frac{A}{X_0 N_A}\left[1 - \frac{4}{3}x\,(1-x)\right] \tag{2.2}$$

N_A labels Avogadro's number and x and $(1-x)$ are the energy fractions transferred to the electron and positron, respectively. As one can see in Figure 2.4 the expression is symmetrical between x and $(1-x)$ since no particle type is preferred.

Integration of equation (2.2) yields the total e^+e^- pair production cross section which is valid for high energies.

$$\sigma = \frac{7}{9}\left(\frac{A}{X_0 N_A}\right) \tag{2.3}$$

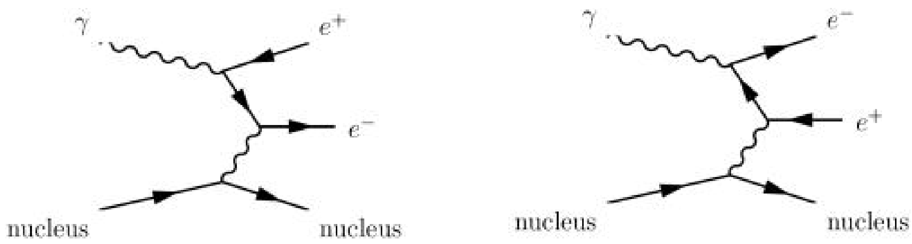

Figure 2.3: Feynman diagrams for pair creation [4]

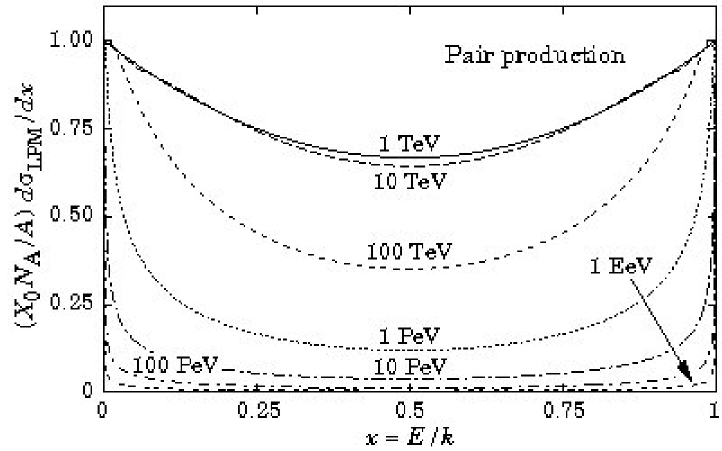

Figure 2.4: Normalized differential cross section for pair production versus energy fraction x of the electron (positron) [5]

This leads to the probability of pair production for a photon penetrating a medium with density ρ to a depth t.

$$P = 1 - \exp\left(-\frac{7}{9}\frac{t \cdot \rho}{X_0}\right) \tag{2.4}$$

In a simulation the photon conversion probability can be determined by counting the number of initial and converted photons.

$$P_{sim} = \frac{\#\ \text{converted}\ \gamma}{\#\ \text{initial}\ \gamma} \tag{2.5}$$

If the energy of the created electron or positron is high enough, it emits new photons due to bremsstrahlung effects discussed in Section 2.2.2. In case these photons convert as well, this results in electromagnetic cascades.

As pair production is dominant for energies larger than a few MeV it is the most relevant process for energy loss of photons created in LHC collisions. Therefore, the interaction especially of electrons and positrons with matter is of interest, too.

2.2 Interaction of electrons and positrons with matter

Charged particles interact with the penetrated matter in several ways depending on their energy (see Figure 2.5). At low energies the dominant process is *ionization* in which the charged particle excites (or frees) an electron of the bound shell of an atom. For this scenario the energy loss increases logarithmically with the passing particle energy so that above a few tenth of MeV, *bremsstrahlung* is more likely as the energy loss is roughly proportional to the particle energy.

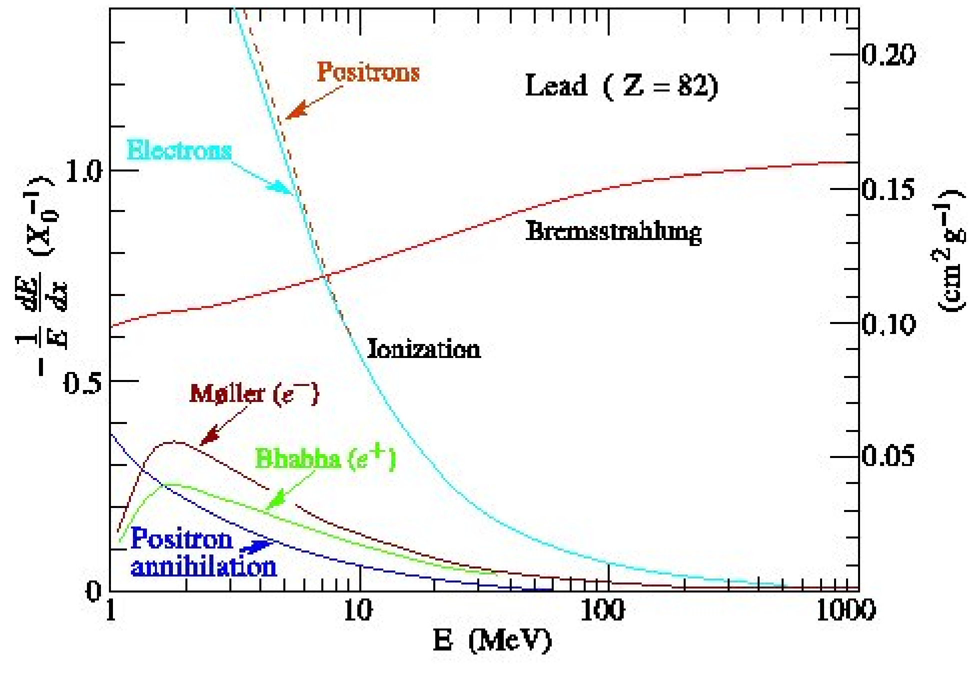

Figure 2.5: Normalized energy loss in units of radiation length in lead versus electron energy [5]

Figure 2.5 shows furthermore that for low energies the scattering processes *Møller scattering* and *Bhabba scattering* as well as *electron-positron-annihilation* contribute little to the total energy loss. Their Feynman diagrams are shown in Figure 2.6.

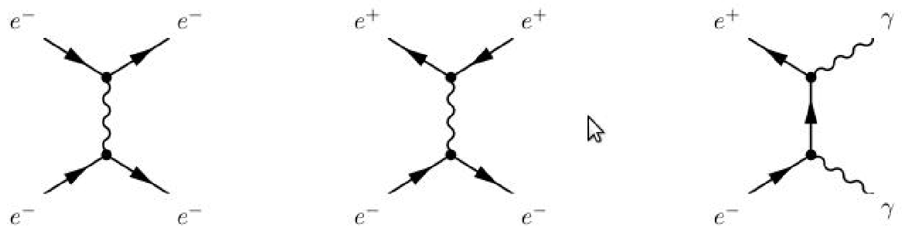

Figure 2.6: Feynman diagrams for scattering processes at low electron (positron) energy Møller scattering (left), Bhabba scattering (middle), e^+e^- annihilation (right) [4]

2.2.1 Ionization

The average energy loss of electrons due to ionization can be approximated by the Bethe-Bloch formula [6].

$$-\frac{\mathrm{d}E}{\mathrm{d}x} = 4\pi N_A r_e^2 m_e c^2 \cdot \frac{Z}{A} \cdot \frac{1}{\beta^2}\left[\ln\left(\frac{\gamma m_e c^2}{2I}\right) - \beta^2 - \frac{\delta}{2}\right] \tag{2.6}$$

Here m_e, r_e and β are the mass, the classical radius and the relativistic velocity $\frac{v}{c}$ of the electron and the quantities Z, A and I characterize the absorber medium as its atomic number, mass number and its mean excitation energy roughly given as $I \approx 16 \cdot Z^{0.9}\text{eV}$ for $Z > 1$ [6]. γ labels the Lorentz factor $\gamma = \frac{1}{\sqrt{1-\beta^2}}$. The parameter δ takes into account that the electromagnetic field of the electron is shielded by the charge density of the electrons of the absorber material.

The energy loss of the electron decreases with $\frac{1}{\beta}$ for small γ and reaches a minimum at $E_{min} \approx 3m_ec^2$. This drop results from the increasing velocity of the particles which leads to less interaction time with the medium. For higher energies $E > E_{min}$ the slope increases proportional to $\ln(\gamma)$. This is due to relativistic effects which allow atoms further away to interact with the traversing particle. For high energies the curve saturates in Fermi-plateau described mathematically by $\delta = \delta(\gamma)$.

2.2.2 Bremsstrahlung

Above a few tenth of MeV bremsstrahlung is the main reason of energy loss. Charged particles are decelerated in a Coulomb field and therefore emit photons. For electrons, the energy loss due to bremsstrahlung is described by Bethe and Heitler who considered energy loss in the electric field of the interaction and of further nuclei and in the electric field of atomic electrons.

The ratio z of the final energy over the initial energy is used in the probability density function [7] which also depends on the depth t (in units of the radiation length) to which an electron has penetrated the medium.

$$f(z) = \frac{(-\ln(z))^{(t/\ln(2)-1)}}{\Gamma\left(\frac{t}{\ln(2)}\right)} \tag{2.7}$$

In principal, this formula does not apply for positrons as the interaction with the atomic electrons is different.

2.2.3 Transition radiation and Cherenkov radiation

There are two other radiation processes that do not contribute significantly to the total energy loss but that are interesting for high-energy particle identification. Firstly, *transition radiation* is emitted when a charged particle traverses the boundary between two media which have different dielectric constants. As the electromagnetic field of a charged particle is influenced by the optical properties of the surrounding medium, it adapts to the new situation by emitting photons mainly in the forward direction. The distribution of the total energy loss by transition radiation peaks at an angle characteristically $\frac{1}{\gamma}$ with respect to the particle direction with the Lorentz factor $\gamma = \frac{E}{mc^2}$ [5]. Therefore, measuring the transition radiation allows to identify particles. This method is used in the ALICE Transition Radiation Detector (see Section 3.1).

In contrast to this, *Cherenkov radiation* is created if a charged particle travels through an homogeneous medium having a velocity larger than the speed of light: $\beta c > c_{medium}$. The photons are emitted under an angle θ_C for which holds: $\cos(\theta_C) = \frac{1}{n\beta}$ with the index of refraction n of the medium [5]. Because of this, Cherenkov radiation allows to identify particles as it is done bye the ALICE High Momentum Particle Identification Detector (see Section 3.1).

2.2.4 Multiple Coulomb scattering

If a charged particle travels trough a medium it is often scattered by very small angles in the Coulomb field of several nuclei. Especially for light particles changes in the direction are not negligible. The distribution of the angle with respect to the original direction of the particle is described by the theory of Molière. For small angles it is roughly Gaussian but for larger angles ($\theta >$ few θ_0 as defined below) collisions with nuclei are more likely than expected from the Gaussian distribution and the shape behaves like Rutherford scattering [5].

$$\theta_0 = \theta_{\text{plane}}^{\text{rms}} = \frac{1}{\sqrt{2}}\theta_{\text{space}}^{\text{rms}} \tag{2.8}$$

The definition of θ_0 leads to a Gaussian approximation with the width

$$\theta_0 = \frac{13.6\text{ MeV}}{\beta cp} z \cdot \sqrt{\frac{x}{X_0}} \cdot \left[1 + 0.038 \cdot \ln\left(\frac{x}{X_0}\right)\right] \tag{2.9}$$

which is valid for the central 98% of the projected angular distribution with an accuracy of 11% or better for $10^{-3} < x/X_0 < 100$ in the case of a single charged particle $|z| = 1$ with velocity $\beta c = c$ (momentum p) for all materials [5]. x/X_0 is the thickness of the medium in units of radiation length.

3 The LHC Experiment

Currently, the particle collider with the highest energy in the world is the *Large Hadron Collider* (LHC) at CERN, Geneva. It is possible to reach a center of mass energy of $\sqrt{s} = 14$ TeV for proton-proton collisions and $\sqrt{s_{NN}} = 5.5$ TeV for lead-lead collisions. The LHC tunnel is circular with a circumference of 26.7 km and was originally built for the Large Electron-Positron Collider (LEP) whose programs ran until 2000. Since the accelerated beams are counter-rotating the LHC has two separate beam lines and it uses four of the eight possible interaction regions provided by the LEP tunnel.

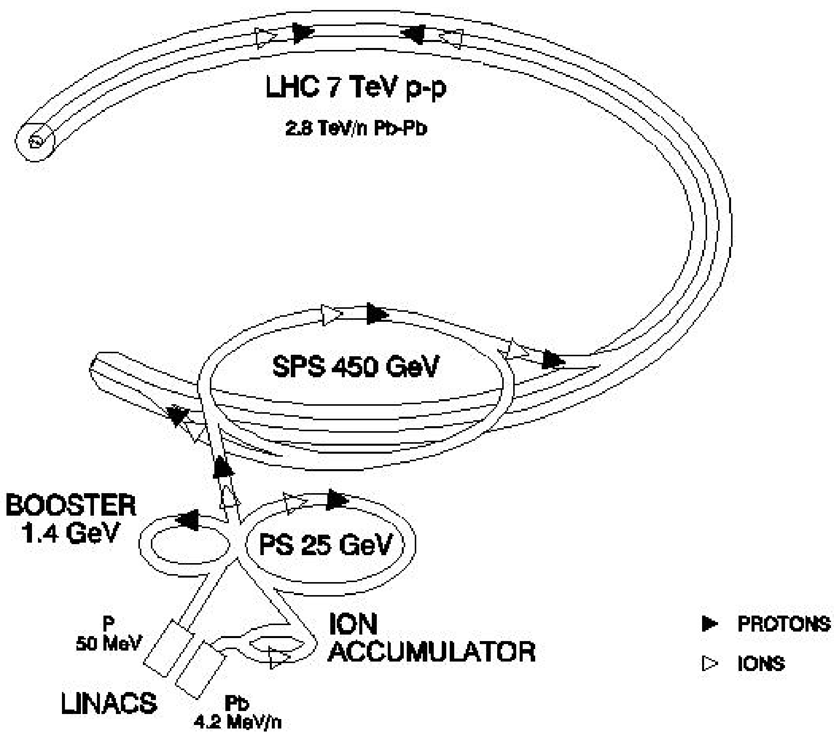

Figure 3.1: The LHC injector complex [8]

The injection chain shown in Figure 3.1 consists of the LINAC2, the Proton Synchrotron Booster (SPB), the Proton Synchrotron (PS) and the Super Proton Synchrotron (SPS) for protons so that finally the particles enter the LHC with an energy of 450 GeV. For ions only the two first steps are different namely the LINAC3 and an ion accumulator which provides cooling.

The four main experiments located at these interaction regions have different physic programs and therefore different designs (see Figure 3.2).

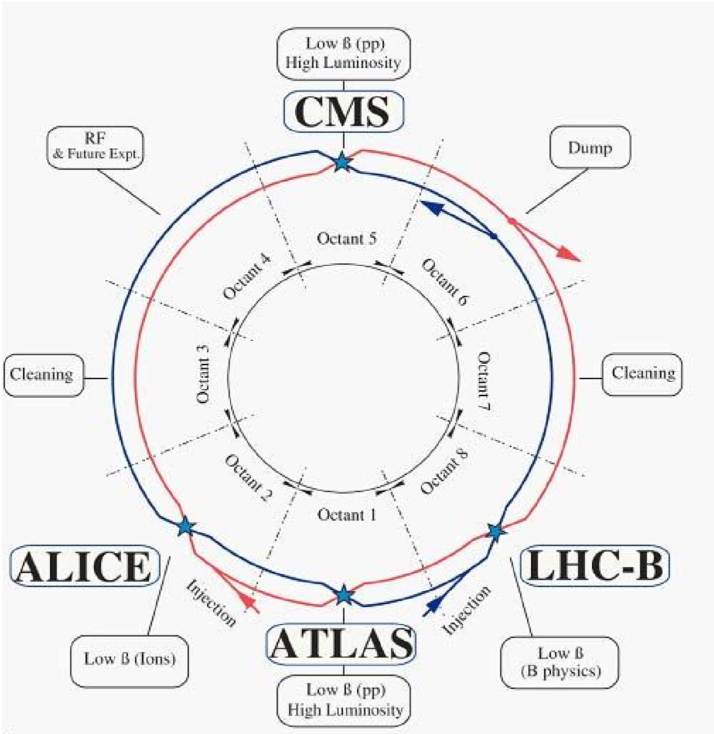

Figure 3.2: Schematic setup of the LHC [8]

- **ATLAS** A Toroidal LHC ApparatuS is designed to cover a wide range of physics. The main topics are the investigation of the Higgs boson and of supersummetric particles which could give information on dark matter as well as the search for extra dimensions [9].
- **CMS** The Compact Muon Solenoid is, besides ATLAS, the second general purpose detector. Therefore the physics program is the same, only the technical design differs.
- **LHCb** The Large Hadron Collider beauty has a focus on the differences between matter and antimatter. With the aim to explain the current amount of matter in the universe LHCb considers theories beyond the Standard Model and concentrates on the CP violation and the decay of beauty and charm hadrons [10].

- **ALICE** A Large Ion Collider Experiment is constructed to analyze heavy ion collisions in addition to proton-proton collisions so as to receive information on strongly interacting matter and the quark gluon plasma.

3.1 The ALICE detector

The main components of the ALICE detector are shown in Figure 3.3. The innermost part, the **Inner Tracking System (ITS)**, consists of six layers of silicon detectors (see zoomed part in Figure 3.3) which are at radial positions between 3.9 cm and 43.0 cm from the beam pipe [11]. With the aim to receive high spatial resolution for primary and secondary vertex reconstructions and to measure particles with low transverse momentum, $p_T < 200$ MeV/c, the material budget is optimized to be 8% of the radiation length X_0. Furthermore, the ITS can be used to enhance the momentum and angular resolution of the TPC and to gain information about processes happening in its dead areas.

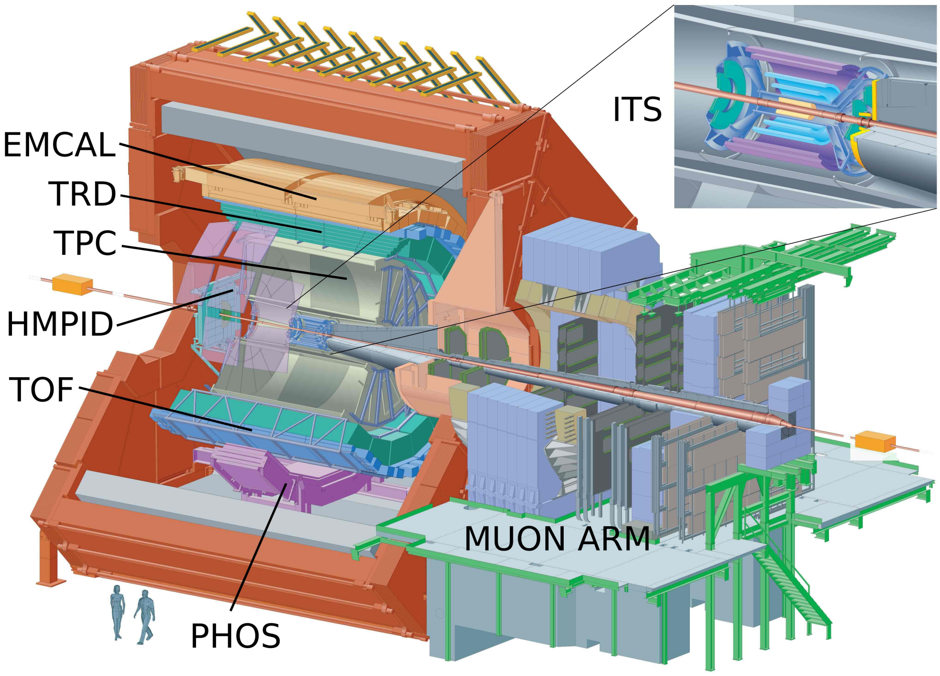

Figure 3.3: Main components of the ALICE detector [12]

The **Time Projection Chamber (TPC)** located at a radial distance from 84.4 cm to 246.6 cm surrounds the ITS. It has a length of about 500 cm in beam direction which corresponds to a pseudo-rapidity range of $|\eta| < 0.9$ [11]. The TPC is a gaseous detector which provides tracking information for multiplicities up to 8000 per rapidity unit. In addition, momentum measurements over a large range, approx. 0.1 GeV/c $\leq p_T \leq$ 100 GeV/c, are possible for charged particles as well as the determination of the specific energy loss dE/dx which allows particle identification for transverse momenta up to 1 GeV/c.

Another important component for particle identification is the **Time Of Flight detector (TOF)**. Measuring the time a particle needs to fly from the interaction point to the detector and combining the data with the track and vertex information taken from the ITS and the TPC, the mass of a particle can be computed for intermediate momentum ranges of 0.5 GeV/c $\leq p_T \leq$ 3.0 GeV/c, 0.5 GeV/c $\leq p_T \leq$ 4.0 GeV/c and 0.3 GeV/c$p_T \leq$ 0.5 GeV/c for pions and kaons, protons and electrons respectively [11].

In contrast to this, the **Transition Radiation Detector (TRD)** is designed to separate electrons from charged pions over a large momentum range above 1 GeV/c because charged pions largely contribute to the background. This is done by analyzing the energy loss and the transition radiation of particles traversing different dielectric media. Moreover, the TRD provides triggering information. Auxiliary, the **High Momentum Particle Identification Detector (HMPID)** identifies hadrons beyond the momentum interval covered by the energy loss measurements of the inner detectors.

The ALICE detector consists of two electromagnetic spectrometers: the **PHOton Spectrometer (PHOS)** and the **ElectroMagnetic Calorimeter (EMCal)**. They are located nearly opposite in azimuth to each other. PHOS is designed to analyze thermal and low-p_T direct photons coming from the initial phase of a collision and jet quenching. The EMCal is a Pb-scintillator focused on the full reconstruction of jet quenching over a large kinematic range. Additionally, the EMCal makes triggering information available.

The muon arm describes a spectrometer in the pseudo-rapidity region $-4.0 \leq \eta \leq -2.5$ [11]. It is used to investigate the μ decay channel of heavy mesons which are especially expected for nucleus-nucleus collisions.

During the next long shutdown in 2018 the **ITS will be upgraded** so that the ability of the readout of 50 kHz interactions for lead-lead runs and 2 MHz for proton-proton runs is guaranteed. For this thesis it is of interest that the material budet will be significantly reduced: using monolithic active pixel sensors reduces the material budget of each of the seven detector layers by a factor of 7 ($X_0 = 0.3\%$ per detector layer) and the one of electrical power and cabling is reduced by a factor of 5 [13]. All in all, this improves the tracking performance especially at low p_T, the momentum resolution and the vertexing.

Since the beam pipe gets smaller, the first layer will be located at a radial distance of 22 mm. But the outermost layer will again be at 430 mm radial distance so that the free space between ITS and TPC remains as shown in Figure 3.3.

4 Analysis

For my analysis I assume that the converter is cylindrically shaped and that it is built in symmetrically around the beam pipe with an inner radius of 60 cm between ITS and TPC. The position is nearly predefined as there is not much space left in the setup of the detector and as the electrons and positrons shall be tracked in the TPC. The length in beam direction is the same as for the TPC so that the covered pseudo-rapidity range is identical $|\eta| < 0.9$ (as described in Section 3.1). Choosing copper as material the radiation length is given as $X_0 = 12.86$ g/cm^2 [2].

In this analysis three different thicknesses t of the converter are investigated, namely $t = 0.025$ cm, $t = 0.100$ cm and $t = 0.150$ cm which yield a conversion probability of 2.4%, 6.9% and 9.7%, respectively. These values are similar to the actual photon conversion probability of roughly 8.5% to 9% in pp collisions at $\sqrt{s} = 7$ TeV.

Neutral pions are the main photon source because they are created in large number in collisions at LHC and decay into two photons with a branching ratio of 98.8% [5]. These photons interact with the medium and perform partly pair production so that in general the distribution of the invariant mass of the reconstructed π^0 contains information about the energy loss of the created electrons and positrons, the conversion probability of photons and the reconstruction efficiency of photons and neutral pions. These quantities all depend on the material budget of the relevant part of the converter and are therefore considered in the following analysis.

I will start with investigating the photon conversion probability for the three chosen thicknesses using a full Monte-Carlo simulation. Since especially the behavior of the electrons is interesting for a reconstruction procedure, a Monte-Carlo simulation is compared to the result of a much faster simulation based on the Bethe-Heitler description of the total energy loss of electrons. The comparison shows a good agreement of those two analysis frameworks and that the energy loss for electrons and positrons under the given conditions is the same. This allows to use the fast simulation in an extended analysis to roughly estimate the reconstruction efficiency of neutral pions. The distribution of the invariant mass of the neutral pion is analyzed in a range in which the signal can be clearly differentiated from background.

4.1 The photon conversion probability

To analyze the photon conversion probability for different thicknesses a Monte-Carlo simulation of GEANT 3 is used. The interface is provided by the *TVirtualMC* class of the CERN framework *root*. Several features had to be implemented like the converter geometry and its properties described above. Photons are created as primary particles in the center of the detector while the transverse momentum p_T is distributed uniformly between 0 GeV/c and 10 GeV/c. Assuming furthermore a flat distribution of firstly, the pseudo-rapidity η in the range from -0.9 to 0.9 and secondly, the azimuthal angle ϕ between 0 and 2π all kinematic properties of the photon are given:

$$\theta = 2 \cdot \arctan\left(-\exp(\eta)\right), \qquad \text{polar angle} \tag{4.1}$$

$$E = |p| = p_T \cdot \cosh(\eta), \qquad \text{energy and absolute momentum} \tag{4.2}$$

$$p_x = p_T \cdot \cos(\phi), \qquad \text{momentum coordinate in x-direction} \tag{4.3}$$

$$p_y = p_T \cdot \sin(\phi), \qquad \text{momentum coordinate in y-direction} \tag{4.4}$$

$$p_z = p_T \cdot \sinh(\eta), \qquad \text{momentum coordinate in z-direction} \tag{4.5}$$

The conversion probability is given by the number of converted photons divided by the number of initial photons as described in equation 2.5. The results are plotted in 25 MeV/c bins of p_T.

Figure 4.1 shows the results of the simulation. The shape is similar for all three thicknesses: At low p_T the conversion probability increases approximately up to $p_T \approx 1.0$ GeV/c. This is due to the total pair production cross section which rises up to $p_T \approx 1.0$ GeV/c as one can see in Figure 2.1. From $p_T = 1.2$ GeV/c on a constant conversion probability is fitted.

The theoretical expectation of the conversion probability for each thickness can be calculated using equation 2.4 and the density of copper $\rho = 8.96$ g/cm^3 [14].

One has to consider that in the Monte-Carlo simulation photons are created with a pseudo-rapidity η distributed uniformly between -0.9 and 0.9. Due to relation 4.1 this corresponds to the range $\frac{\pi}{4}$ to $\frac{3\pi}{4}$ for the polar angle θ. If the longitudinal momentum component p_z of a photon is not zero it has to travel a longer way through the converter. Therefore, the effective thickness of the converter is larger than t but lower than $\sqrt{2}t$.

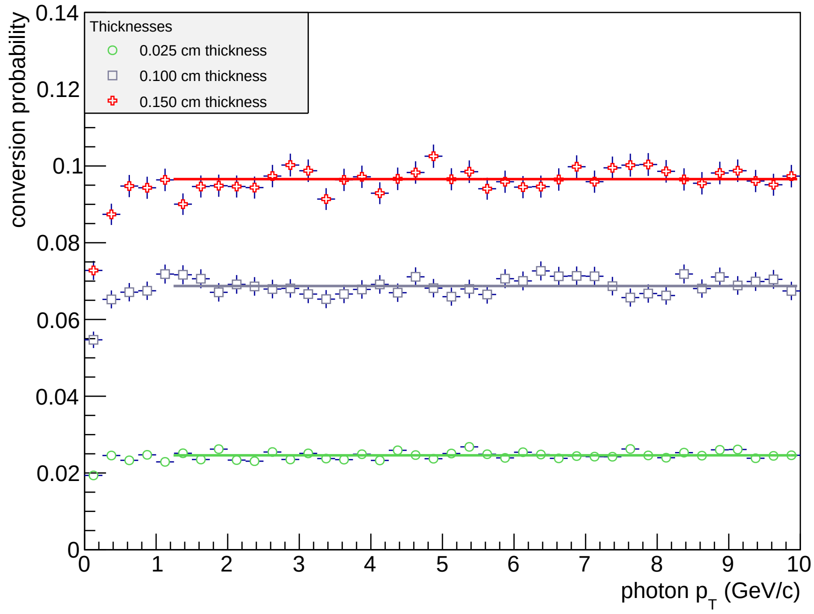

Figure 4.1: Photon conversion probability for different thicknesses of the converter (made of copper $X_0 = 12.86$ g/cm^2) using a Monte-Carlo simulation.
For $p_T \geq 1.2$ GeV/c constant conversion probabilities are fitted.

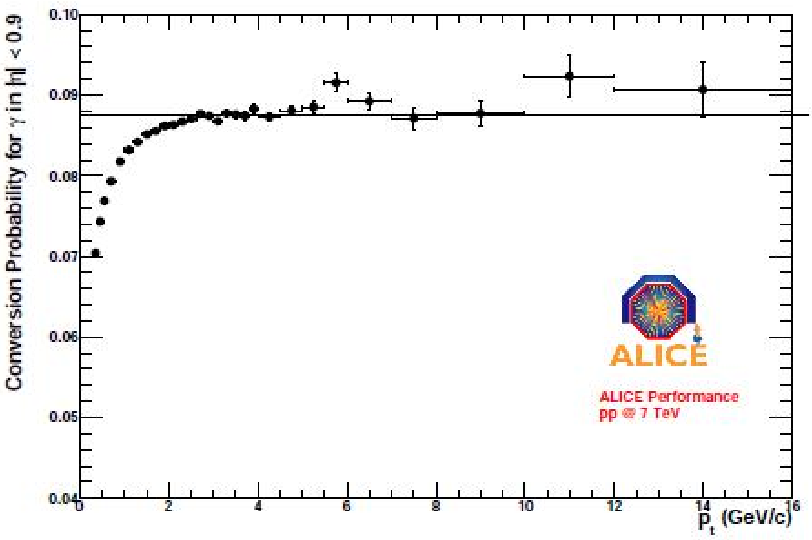

Figure 4.2: Photon conversion probability for pp collisions at $\sqrt{s} = 7$ TeV simulated for ALICE [15]

Simulated thickness	Theoretical conversion probability		Monte-Carlo conversion probability
	t	$\sqrt{\mathbf{2}}\cdot\mathbf{t}$	
$t = 0.025$ cm	1.3%	1.9%	(2.46±0.02)%
$t = 0.100$ cm	5.3%	7.4%	(6.87±0.04)%
$t = 0.150$ cm	7.8%	10.9%	(9.66±0.05)%

Table 4.1: Comparison of the theoretical expectation and the Monte-Carlo fit results for the photon conversion probability for different thicknesses of copper ($X_0 = 12.86$ g/cm^2)

It can be seen that for 0.100 cm and 0.150 cm thickness the Monte-Carlo simulation matches the theoretical expectation.

In addition to this comparison, one can contrast the performed Monte-Carlo simulation with a Monte-Carlo simulation which has the whole ALICE detector implemented and shows the prediction for pp collision at $\sqrt{s} = 7$ TeV for the same η-range: $|\eta| < 0.9$ (Figure 4.2). A distinct difference is visible in the sloping curve which rises for higher p_T, approximately up to $p_T \approx 2.5$ GeV/c in the ALICE detector simulation. This is due to the material properties. Whereas for the converter copper is simulated the ALICE photon conversions happen basically due to the material of the ITS of which the most relevant components are the six silicon detectors [11]. The photon conversion probability saturates for silicon at higher p_T than for copper because the cross section depends on the material properties for low p_T, thus on X_0. Therefore, copper provides an advantage for the photon conversion method in the range of approximately $p_T = 1.0$ GeV/c to $p_T = 2.5$ GeV/c.

The material budget of the ITS in the ALICE detector yields 7.26% of X_0 in total [11] which is larger than 6.9% of X_0 ($t = 0.100$ cm) and smaller than 10.5% of X_0 ($t = 0.150$ cm). This corresponds to the fact that the ALICE conversion probability is in between the simulated one of those two thicknesses. For higher transverse momenta one can see larger errors in the ALICE detector simulation which corresponds to less statistics since high energy photons are less probable in the considered collisions. This feature cannot be seen in the Monte-Carlo simulation of the converter as the distribution of the transverse momentum is flat.

4.2 Comparison of the energy loss of electrons using a fast and a Monte-Carlo simulation

In order to compare the results of the energy loss of the Monte-Carlo simulation to a faster one electrons are chosen as primary particles in GEANT having a fixed transverse momentum of 1 GeV/c. Their energy in front of and behind the converter determines the relative final energy $\frac{E_{\text{behind}}}{E_{\text{in front of}}}$. The same quantity is obtained by a fast simulation of electrons which lose their energy according to the Bethe-Heitler distribution described by equation 2.7 using the same thickness $t = 0.15$ cm as for the converter. The normalized distributions of the relative final energy shown in Figure 4.3 have a similar shape. But a relative final energy larger than $\approx 97\%$ (energy loss smaller than $\approx 3\%$) is more probable in the GEANT simulation and vice versa. The deviation occurs as in GEANT more features are considered, especially scattering processes.

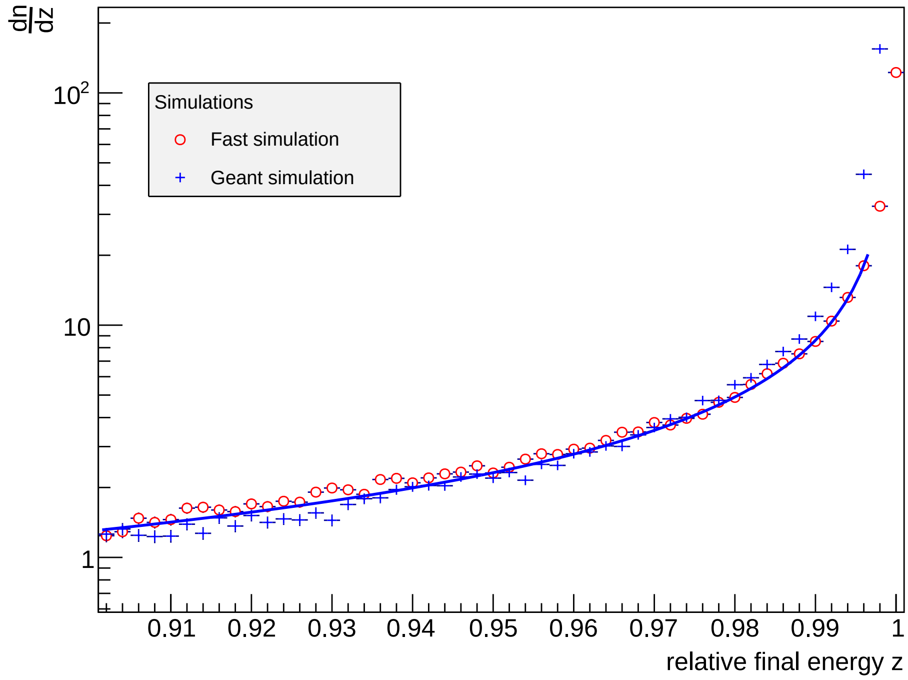

Figure 4.3: Normalized distributions of the relative final energy of electrons generated by a Monte-Carlo simulation (blue) and a fast simulation (red) which is based on the Bethe-Heitler energy loss

The blue line shows the fit of the Monte-Carlo data with the Bethe-Heitler formula 2.7 which matches most of the data points. This means that bremsstrahlung is the main reason for energy loss. The fit range is chosen up to a final relative energy of 0.997 because the fit function diverges for $z \to 1$. This yields the fit parameter $t_{\text{fit}} = (0.135 \pm 0.001)$ which can be interpreted as an effective thickness. This value is larger than the radial thickness $t_{\text{true}} = \frac{t \cdot \rho_{Cu}}{X_0^{MC}} = 0.105$ of the converter in units of the radiation length but smaller than the maximal thickness $\sqrt{2} t_{\text{true}} = \sqrt{2} \frac{t \cdot \rho_{Cu}}{X_0^{MC}} = 0.148$ which is valid for particles with $|\eta| = 0.9$.

In theory, the Bethe-Heitler formula does not apply for positrons because they interact differently with the medium. Hence, the energy loss for positrons is contrasted using the same Monte-Carlo simulation. In Figure 4.4 the distribution for positrons minus the distribution for electrons is plotted. As a result there is no significant difference between electron and positron interaction under given conditions.

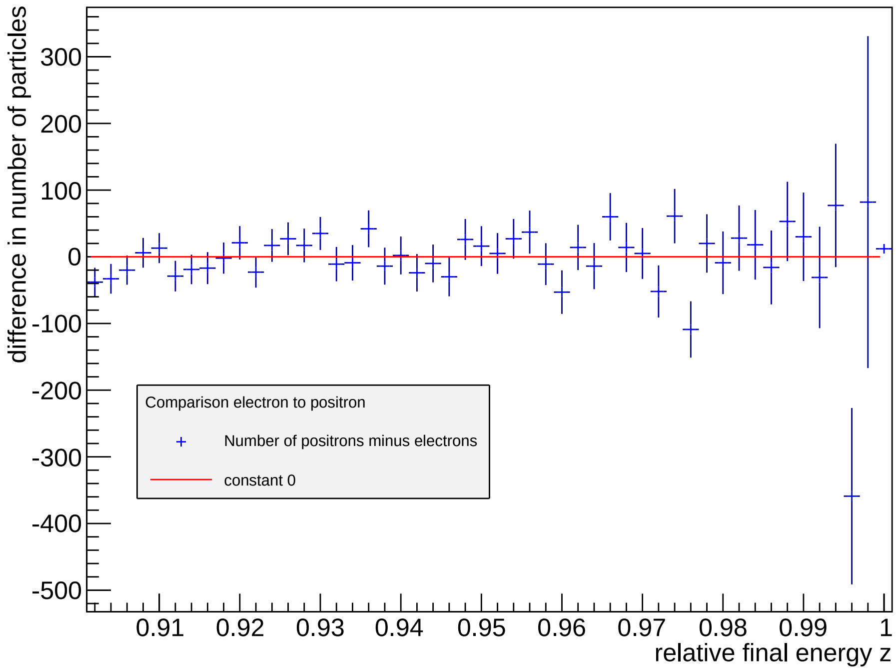

Figure 4.4: Positron minus electron distribution of the energy loss in 0.10 cm copper ($X_0 = 12.86$ g/cm^2) using a Monte-Carlo simulation

So all in all, the Bethe-Heitler formula can be used as description of the energy loss due to the converter in the fast simulation replacing t in equation 2.7 by the fit paramter t_{fit} for 0.15 cm thickness.

4.3 Invariant mass of π^0

In order to analyze the impact of the different thicknesses on the reconstruction of the neutral pions the fast simulation generates neutral pions as primary particles with a fixed transverse momentum. In the simulation each π^0 decays into two photons. Furthermore, each photon converts where an energy fraction x of the photon energy is assigned to the electron according to the probability density function $P(x) = 1-\frac{4}{3}x(1-x)$. The positron receives the remaining energy $(1 - x)$. At this point, the energy loss of the leptons is calculated and subtracted using the Bethe-Heitler equation 2.7. The procedure of sampling this distribution is described in Section 4.3.1. Considering a converter with 0.150 cm thickness an appropriate effective thickness t_{eff} (in units of the radiation length) is given by the fit parameter t_{fit} of Section 4.2. For the other thickness of the converter the effective thickness t_{eff} is scaled by the ratio of the converter thickness over the reference value as shown in Table 4.2. These values are taken as parameters for the Bethe-Heitler equation which means that the path length for electron and positron through the converter is constant.

Converter thickness		**Effective thickness**
[cm]	in units of X_0	in units of X_0
0.025	0.017	0.023
0.100	0.070	0.090
0.150	0.104	0.135

Table 4.2: Comparison of the simulated converter thickness in (cm) and units of the radiation length to the effective thickness due to a GEANT fit with the Bethe-Heitler formula

The distribution of the invariant mass of the π^0 is plotted in Figure 4.5 for different thicknesses and initial transverse momentum $p_t = 1$ GeV/c. The invariant mass of the π^0 is 0.135 GeV/c^2 [5]. As described in [16] one can assume that the peak can be separated from the background in a range from 0.100 GeV/c^2 to 0.140 GeV/c^2. Hence, the fraction of the simulated pions in the signal region can be calculated as shown in Table 4.3. Low energy particles lose energy more easily and the energy loss increases with the thickness as well.

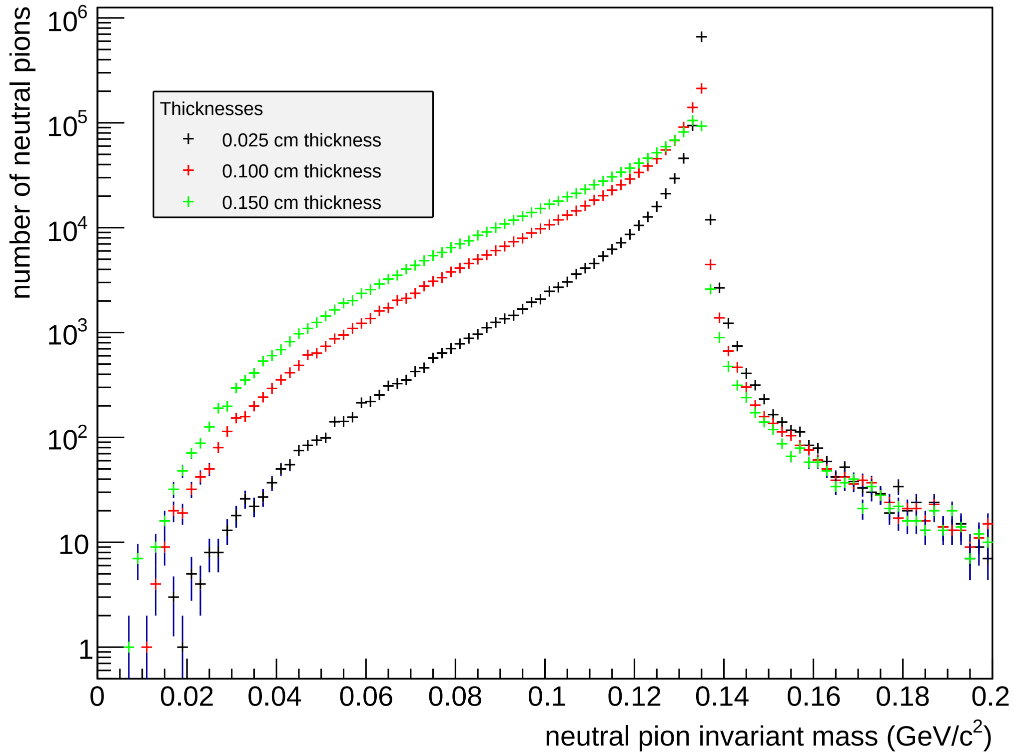

Figure 4.5: Invariant mass distribution for photon pairs from the π^0 decay created by a fast simulation based on the Bethe-Heitler energy loss for electrons The initial π^0 momentum is 1 GeV/c.

Thickness (cm)	$\mathbf{p_T}$ = 0.5 GeV/c	$\mathbf{p_T}$ = 1 GeV/c	$\mathbf{p_T}$ = 5 GeV/c	$\mathbf{p_T}$ = 10 GeV/c
0.025	93.4%	95.3%	97.0%	97.2%
0.100	85.3%	87.3%	89.0%	89.2%
0.150	78.3%	80.4%	82.1%	82.3%

Table 4.3: Fraction of events in the signal region 0.100 GeV/c^2 $\leq m_{\pi^0} \leq$ 0.140 GeV/c^2 for different thicknesses and initial transverse momenta p_T of π^0

The reconstruction efficiency of the π^0 depends above all on the photon conversion probability which has been analyzed in Section 4.1 and the tracking efficiency of the TPC which is 90% for charged particles with a transverse momentum larger than 1 GeV/c. In a rough estimation the values of Table 4.3 are multiplied with the probability of two photons to convert and four leptons to be tracked. Assuming a track finding efficiency of 0.9 for each lepton this yields better results for higher initial transverse momentum.

Thickness (cm)	**Conversion probability**	**Reconstruction efficiency of π^0 for initial momentum p_T**			
		0.5 GeV/c	1 GeV/c	5 GeV/c	10 GeV/c
0.025	2.41%	0.04%	0.04%	0.04%	0.04%
0.100	6.87%	0.26%	0.27%	0.28%	0.28%
0.150	9.66%	0.48%	0.49%	0.50%	0.50%

Table 4.4: Estimated reconstruction efficiency of the π^0 in dependence on different thicknesses and initial transverse momenta p_T

It is obvious that both features largely influence the reconstruction efficiency which is estimated to a few per mill. Furthermore, these values do not depend on the momentum and energy resolution of the detector.

4.3.1 Determination of random energy ratio z according to the Bethe-Heitler distribution

The main idea of generating random numbers according to a given distribution $f(z)$ is the following: firstly, one chooses a random number r between zero and one. After that, one has to make sure that the function $f(z)$ is normalized. Then, the random number z_R is given by the value for which the integral of the distribution equals r.

Often the determination of z_R from r cannot easily be done. This is the case for the Bethe-Heitler equation (2.7).

$$f(z) = \frac{(-\ln(z))^{(t/\ln(2)-1)}}{\Gamma\left(\frac{t}{\ln(2)}\right)}$$

In principal, one has to evaluate equation 4.6.

$$r = \int_0^{z_R} \frac{(-\ln(z))^{(t/\ln(2)-1)}}{\Gamma\left(\frac{t}{\ln(2)}\right)} \mathrm{d}z \tag{4.6}$$

But a trick can be used (taken from [7]). Equation 4.6 can be transformed by defining $x = -\ln(z) \quad \Rightarrow \mathrm{d}z = -\exp(-x)\mathrm{d}x$. The range $0 \leq z \leq z_R$ corresponds therefore to $-\infty \leq x \leq x_R$ with $x_R = -\ln(z_R)$. This yields equation 4.7.

$$r = \int_{-\infty}^{x_R} -\frac{x^{(t/\ln(2)-1)} \exp(-x)}{\Gamma(t/\ln(2))} \mathrm{d}x \tag{4.7}$$

The integrant of 4.7

$$g(x) = \frac{x^{(t/\ln(2)-1)} \exp(-x)}{\Gamma(t/\ln(2))} \tag{4.8}$$

is a special case of the Gamma distribution $g'(x;\lambda,k)$ with $\lambda = 1$ and $k = t/\ln(2)$.

$$g'(x;\lambda,k) = \frac{x^{(k-1)} \lambda^k \exp(-\lambda x)}{\Gamma(k)} \tag{4.9}$$

This is an advantage as in the *root* library *MathMore* the sampling of the Gamma distribution is provided. Hence, a random number x_R can be generated according to the Gamma distribution with shape parameter $k = t/\ln(2)$ and scale parameter $\lambda = 1$. From this, z_R can be calculated using $z_R = \exp(-x_R)$.

5 Summary and Outlook

In this thesis a cylindrical photon converter made of copper has been simulated having an inner radius of 60 cm and thickness of 0.025 cm, 0.100 cm or 0.150 cm. As it is dedicated to preserve the photon conversion method after the replacement of the ITS during the long shutdown in 2018 different properties have been investigated.

Using GEANT the photon conversion probability has been computed for the different thicknesses as listed in Table 5.1. Except for the smallest thickness the values are compatible to theoretical expectations given by formula 2.4. A comparison with a simulation of the actual ALICE setup shows that for copper the photon conversion probability saturates at lower transverse momentum, namely $p_T \approx 1$ GeV/c. This is an advantage regarding the photon conversion method.

Furthermore, the energy loss of electrons and positrons has been analyzed. Therefore, both particle types have been simulated separately as primary particles in GEANT. The distributions of the ratio of final to initial energy z have been subtracted which has shown that there is no significant difference in the behavior of electrons to positrons under given conditions.

Within my bachelor thesis it was not possible to run a full Monte-Carlo simulation for each quantity of interest. Thus, the quality of a fast simulation was of interest which is based on the Bethe-Heitler equation 2.7. This is a distribution of the ratio of final over initial energy z and it describes the energy loss of electrons due to bremsstrahlung depending on the material thickness t in units of the appropriate radiation length. The comparison of the z distribution of electrons between both simulations shows a good agreement.

That is why the fast simulation shall be used in addition to GEANT for further investigations. As a first step an effective thickness for 0.150 cm copper has been derived by fitting the Monte-Carlo distribution with the Bethe-Heitler equation. The fit parameter is $t_{\text{fit}} = 0.135 \pm 0.001$. This value has been scaled to get effective thicknesses for 0.100 cm and 0.025 cm copper as well (see Table 5.1). These values have been used in the Bethe-Heitler equation of the fast simulation for the further analyses.

In a last step the distribution of the invariant mass of neutral pions has been simulated with the fast simulation. Regarding the assumption that the signal in a range of 0.100 GeV/c^2 to 140 GeV/c^2 contrasts from the background the fraction of events in the signal region can be determined and afterwards scaled by multiplying with $c = p_{\text{conv}}(t)^2 \cdot 0.9^4$. The factor c includes the $t-$dependent probability $p_{\text{conv}}(t)$ that both photon coming from the π^0 convert and four times the tracking efficiency of the TPC which is 0.9 for particles with a transverse momentum larger than 1 GeV/c. The estimated reconstruction efficiencies are shown in Table 5.1.

Simulated thickness	**Conversion probability** (Monte-Carlo)	**Effective thickness** (used in fast simulation)	**Reconstruction efficiency** $\boldsymbol{\pi^0}$ initial $p_T = 10$ GeV/c
0.025 cm	(2.46±0.02)%	0.023	0.04%
0.100 cm	(6.87±0.04)%	0.090	0.28%
0.150 cm	(9.66±0.05)%	0.135	0.50%

Table 5.1: Overview of the obtained results for three different thicknesses

In further investigations it would be useful to combine both analysis frameworks. The fast simulation can be extended regarding multiple scattering in the material, the momentum resolution of the detector and overall a reconstruction procedure of electrons and positrons to photons and of photons to neutral pions. This is important for simulations of many particles per event which is necessary to get an estimation of the background; for one thing false pairing of the leptons contribute, for another thing pairing with charged pions has to be taken into account as they can be misidentified as electrons or positrons in the detector.

Moreover, additional simulations can be done by GEANT. Simulations on the new ITS can be combined with the results of the converter simulations. Supplementary, the energy and momentum resolution of further particles is important, especially for other experiments. After all, one can decide whether a photon converter which would provide advantages concerning the photon conversion method is compatible with the overall physics program of the ALICE experiment.

Acknowledgements

First of all, I would like to thank PD Dr. Klaus Reygers for supervising me in this thesis and for giving his professional opinion on my work.

Also I am grateful to Daniel Lohner for his support and his ideas how to solve physical and technical problems.

Furthermore, I want to express my gratitude to Dr. Kai Schweda for the invitation to the group and his willingness to evaluate this thesis as second examiner.

My special thanks go to Marc Barra, Halil Cakir, Tobias Denz and Yifei Wang for the pleasant working athmosphere.

Last but not least, I am very grateful to my parents who supported me during my studies and proofread this thesis.

Appendix

List of Figures

List of Tables

References

[1] Takashi Hachiya, *Study of Charm Production from the Measurement of Single Electrons in Au + Au Collisions at* $\sqrt{s_{NN}}$ *= 200 GeV*, 2010.

[2] http://pdg.lbl.gov/2012/AtomicNuclearProperties/HTML_PAGES/029.html, Database of PARTICLE Data Group
last visited: 21.07.2013.

[3] http://www.upscale.utoronto.ca/GeneralInterest/DBailey/SubAtomic/Lectures/LectF05/Photon.gif,
last visited: 06.07.2013.

[4] Friedericke Bock, *ALICE Capabilities for Studying Photon Physics with the Conversion Method at LHC Energies*, 2010.

[5] J. Beringer et al., *PARTICLE Physics Booklet*, Extracted from the "Review of PARTICLE Physics". J. Beringer, et al. (PARTICLE Data Group), Phys. Rev. D 86, 010001 (2012), 2012.

[6] C. Grupen and B. Shwartz, *PARTICLE Detectors*, *Cambridge monographs on particle physics, nuclear physics and cosmology* (2008).

[7] W. Adam, R. Frühwirth, A. Strandlie, and T. Todorov, *RESEARCH NOTE FROM COLLABORATION: Reconstruction of electrons with the Gaussian-sum filter in the CMS tracker at the LHC*, *Journal of Physics G Nuclear Physics* **31** (Sept., 2005) 9.

[8] Lyndon Evans and Philip Bryant, *LHC Machine*, *Journal of Instrumentation* **3** (2008), no. 08 S08001. stacks.iop.org/1748-0221/3/i=08/a=S08001.

[9] T. A. Collaboration, *The ATLAS Experiment at the CERN Large Hadron Collider*, *Journal of Instrumentation* **3** (2008), no. 08 S08003. stacks.iop.org/1748-0221/3/i=08/a=S08003.

[10] T. L. Collaboration, *The LHCb Detector at the LHC*, *JINST, 3:S08005* (2008).

[11] The ALICE Collaboration, *The ALICE experiment at the CERN LHC*, *Journal of*

Instrumentation **3** (2008), no. 08 S08002. stacks.iop.org/1748-0221/3/i=08/a=S08002.

[12] J. Klein, *Commissioning of and preparations for physics with the transition radiation detector in a large ion collider experiment at cern*, 2008.

[13] T. A. Collaboration, *Upgrade of the inner tracking system conceptual design report*, Version: CDR-1, 2012.

[14] http://www.periodensystem.info/elemente,
last visited: 17.07.2013.

[15] K. Aamodt et. al., *π^0 and η meson measurement with conversions in ALICE in proton-proton collisions at $\sqrt{s}$ = 7 TeV, $\sqrt{s}$ = 2.76 TeV and at $\sqrt{s}$ = 900 GeV at the CERN LHC*, 2011.

[16] *ALICE Collaboration* collab., Abelev, B. and others, *Neutral pion and η meson production in proton-proton collisions at $\sqrt{s} = 0.9$ TeV and $\sqrt{s} = 7$ TeV*, *Phys.Lett.* **B717** (2012) 162–172, [arXiv:1205.5724].

*Erklärung

Ich versichere, dass ich diese Arbeit selbstständig verfasst und keine anderen als die angegebenen Quellen und Hilfsmittel benutzt habe.

Heidelberg, den ...,